Gépészet 2008
Budapest, 29-30.May 2008

G-2008-E-15

HYBRID/ZONAL RANS/LES COMPUTATION OF AN AIRFOIL

L. Nagy
Ph.D. student, Department of Fluid Mechanics, Budapest University of Technology and Economics,
H-1111 Budapest, Bertalan L. u. 4-6. Tel: (+36-1) 463-2546, e-mail: nagy@ara.bme.hu

M. M. Lohász
Assistant professor, Department of Fluid Mechanics, Budapest University of Technology and Economics,
H-1111 Budapest, Bertalan L. u. 4-6. 5. Tel: (+36-1) 463-1560, e-mail: lohasz@ara.bme.hu

T. Régert
Assistant professor, Department of Fluid Mechanics, Budapest University of Technology and Economics,
H-1111 Budapest, Bertalan L. u. 4-6. 5. Tel: (+36-1) 463-1560, e-mail: regert@ara.bme.hu

J. Vad
Associate professor, Department of Fluid Mechanics,Budapest University of Technology and Economics,
H-1111 Budapest, Bertalan L. u. 4-6. 5. Tel: (+36-1) 463-2464, e-mail: vad@ara.bme.hu

Abstract: Large-eddy simulations were carried out in the vicinity of the RAF-6E airfoil at incidence of 5° at a chord based Reynolds number of 122 000. Hybrid RANS/LES method was employed on a zonal domain of the airfoil. Appropriate boundary conditions were investigated for the interface between RANS and LES on 2D RANS simulations. In order to determine the required extension of the domain in the spanwise direction, three different grids were prepared. Streamwise velocity components and velocity fluctuations of these numerical simulations were compared with Laser Doppler Anemometry measurements in 10 profiles. Static pressure distribution on the surfaces of the airfoil was compared as well. The computed laminar to turbulent transition zone position was compared with flow visualization techniques.

Keywords: *Zonal, Hybrid, RANS, LES, airfoil*

1. INTRODUCTION

Axial flow fans are widely applied in air-conditioning systems, jet engines, as well as in buildings or traffic vehicles. It has been known for a long time that not just the jet engines but other fans generate noise which can influence the human being or its comfort feeling. This is the reason why research on the fan generated noise was positioned in the focus in the last two decades.

This study will show the middle step of a three steps methodology about a low Reynolds number axial flow fan generated noise reduction, developed at BME Department of Fluid Mechanics (DFM). The first and the second steps of the methodology contain numerical simulation using a computational fluid dynamics (CFD) tool. The previous study [1] prescribed several two-dimensional (2D) Reynolds averaged Navier-Stokes (RANS) based computations, completed with two-equation eddy viscosity turbulence models. Since aeroacoustic phenomena such as the noise produced by a rotating object in a channel [2] is characterized with small fluctuation of flow properties, therefore a fine resolution is required for the flow domain. Concerning the computational effort, large-eddy simulation (LES) is the most appropriate method for predicting the noise sources required for computational aeroacoustics (CAA) and it was applied in this study, even if it is known that LES is not

capable to predict the high frequency range of the generated noise [3]. Nevertheless the direct CAA or direct numerical simulation (DNS) coupled CAA can solve this problem.

The number of references is limited dealing with LES of axial flow fan for further aeroacoustical analyses. Most of them employed in-house developed codes for determining the flow pattern [3, 4, 5]. Only a few research projects are based on coupling commercially available CFD and CAA software such as ANSYS Fluent and LMS SYSNOISE [6].

The blades of an axial flow fan operate in cascade (blade row) arrangement. However, if the solidity (blade chord-to-spacing ratio) of an axial flow blade row is relatively low - as in the case of several industrial fans - the operation of a blade section can be considered to be analogous to that of an isolated airfoil.

[7] described the RANS/LES hybrid method using coupled simulations. It contains a RANS calculation near the solid boundary and a LES simulation farther from them. In the coupled simulation, the interface between the two domains is a source of errors which was investigated e.g. in [8]. The present study combines the RANS and LES approaches in order to take advantage of both methods. The less expensive RANS simulation is applied to determine the main flow. This method is switched to LES to get accurate results in the vicinity of the airfoil, simultaneously reconstructing the unsteady turbulent parameters [9, 10]. In this case, the interface problem is radically simplified, since there is no back coupling from LES to RANS. Choosing the interface between the two processes along prescribed streamlines by RANS and choosing an appropriate boundary condition (BC) on it are a novel concepts to the author best knowledge.

A small spanwise segment of an axial turbomachinery blade was investigated through a case study, related an individual, rectilinear RAF-6E airfoil [11, 12], which is widely applied in turbomachinery (for ventilation and air conditioning) because of its easy manufacturing and acceptable efficiency. It has rounded leading and trailing edges. The present model has a chord length (c) of 200 mm (Figure 1). The radius of the leading edge is 0.0115c and the trailing edge has a radius equal to 0.0076c. This airfoil has a flat pressure side (PS) which enables an accurate definition of the inclination angle, and its easy manufacturing. The computations were validated against in-house measurements with Laser-Doppler Anemometer (LDA) and pressure measurements on the airfoil surfaces. The Reynolds number, based on the chord (c), inlet reference velocity (U_{ref}) and kinematic viscosity (ν) of the air at 20°C was 122 000.

2. DESCRIPTION OF THE MEASUREMENTS

The measurements were carried out in the National Physics Laboratory (NPL) type wind tunnel of DFM. The closed test section of the wind tunnel has a cross section of 500mm height and 505mm width. In the first part of the experimental study, two quantitative measurements were prepared. The LDA was focused to determine the velocity field with the turbulent intensity in the vicinity of the airfoil. More details of this measurements, the position of the airfoil and measurement configurations are described in [1, 13]. The last phase of the validation process regards the pressure measurements, which are described later.

In order to make qualitative validation, some flow visualisation investigations were executed in the NPL type wind tunnel. In the first part of this process, oil flow visualisation was prepared using a mixture of paraffin, instrument oil and titanium-dioxide. A segment of this result is shown in Figure 13/e. As the second step, a laser sheet was used in a section in the middle of the airfoil section suction side (SS) to facilitate the post processing of the oil smoke visualisation. Figure 13/a is taken from this scenario and shows a small separation zone. The pressure measurements were carried out with an in-house developed digital pressure device calibrated to a Betz-type manometer. The relative uncertainty of the digital

pressure device is 2%. The reference pressure was obtained through a pressure tap loop attached to the confusor of the wind tunnel. The error was estimated to around 1%, regarding the ambient temperature, ambient pressure and measured pressure in an error propagation analyses. The pressure measurement positions are described in the caption of Figure 1.

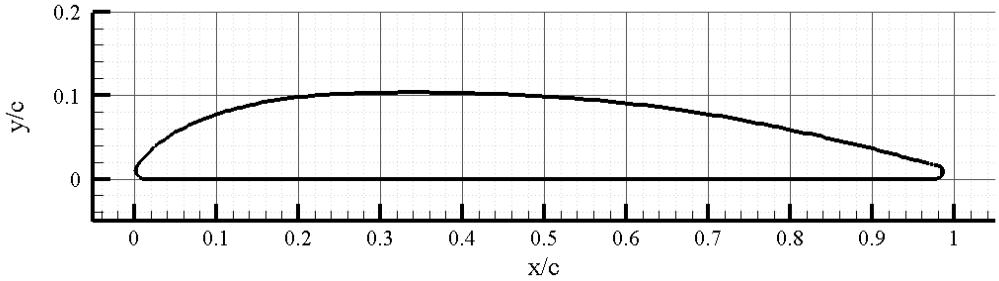

Fig. 1 The section of the RAF-6E airfoil. The pressure measurement positions are at the middle in spanwise direction and at following chord length in the streamwise direction. On the SS: 0, 0.09, 0.19, 0.3, 0.40, 0.52, 0.62, 0.72. On the PS: 0.14, 0.29, 0.44, 0.61, 0.77.

3. CFD DOMAIN

The previous 2D RANS computations were conducted in a domain of 15*c* x 2.5*c* in streamwise and wall-normal direction [1]. The airfoil was positioned according to the wind tunnel measurement. The inlet and outlet boundaries were placed sufficiently far to achieve minimal influence on the flow in the vicinity of the airfoil. The distance between the inlet boundary and the leading edge was set to 5*c*, while the outlet boundary was positioned from the trailing edge at 9*c*. From this simulation, the streamlines have been determined, and were considered as position for the BCs position for the new LES domain. The LES domain has the dimension of 3*c* x 1*c* (Figure 2).

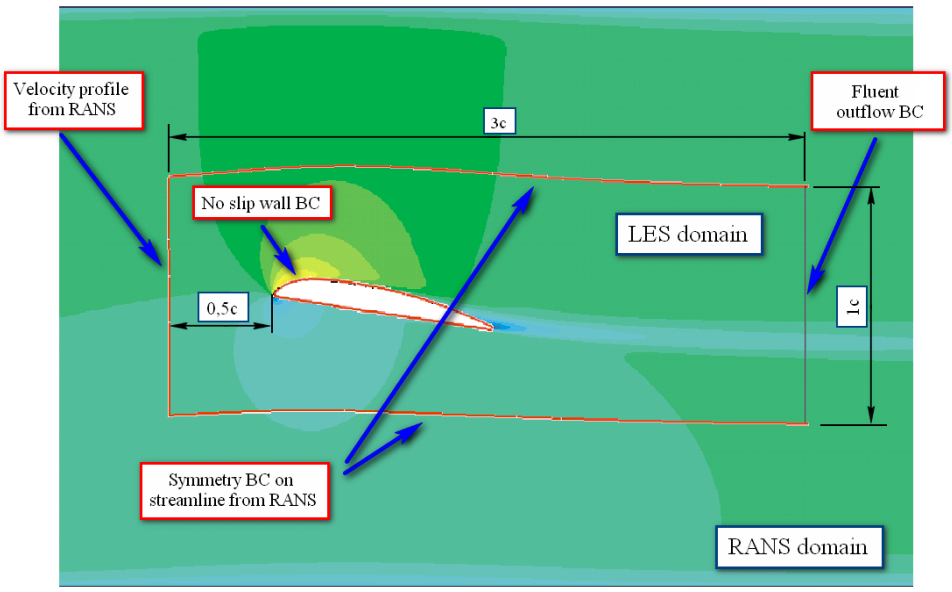

Fig. 2 Zonal/Hybrid method using the LES domain and previous RANS domain

Two different turbulence models were applied from the two equation model family: the (shear-stress transport) SST k-ω low Reynolds number turbulence model and the realizable k-ε model with enhanced wall treatment. The previous RANS simulation [1] using k-ε viscous model provided an appropriate BC for this *zonal* domain. In the present study, this simulation is termed *k-ε RANS*.

3.1 Theory of the domain dimensions

This study is restricted to low Mach number; because the actual Mach number based on the U_{ref} velocity is lower than 0.3. The present methodology is prepared for resolution of noise sources in the upstream, near-airfoil as well as the downstream flow regimes.. Because of the increase of the useful number of cells, the domain has been confined to the vicinity of the airfoil. This method is usually termed herein as the zonal approach of numerical simulation.

To check the possibilities of the BC on LES domain in 2D, several RANS computations were carried out. Table 1 shows the part of the available BCs in ANSYS FLUENT, in the form of *inlet-streamlines-outlet*. This notation is following in Table 1 (in each bracket) and Figure 3. The comparison of the different BCs is shown in Figure 3, for the velocity profile at the outlet. It can be concluded that all of the chosen BC is allowed for the present study. The symmetry BC usually applies for mirror symmetry case but it could be also used when a zero shear slip wall condition would be prescribed. Since the wall BC (moving or stationary) required strict prescription of the fluxes (e.g. mass flow rate) and to produce this condition is not simple, therefore the symmetry condition was applied on the streamlines. Although the pressure outlet BC provided same the results as the outflow BC the further was applied for further simulation since it is more appropriate simulating the vortices leaving the domain.

Inlet	**On streamlines**	**Outlet**
Pressure profile (p)	Moving wall with velocity profile and no slip condition (mwn in Fig 3.)	Pressure (p)
Velocity profile (v)	Moving wall with velocity profile and specified shear stress profile (mws in)	**Outflow (o)**
	Stationary wall with specified shear stress profile (sws)	
	Symmetry (s)	

Tab.1 The part of the possible BC in ANSYS FLUENT

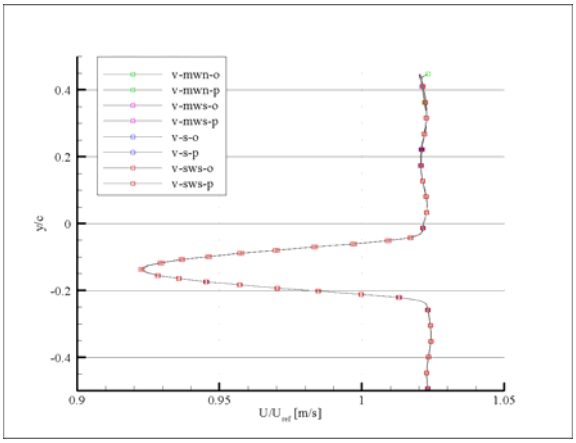

Fig. 3 The velocity profile at the outlet

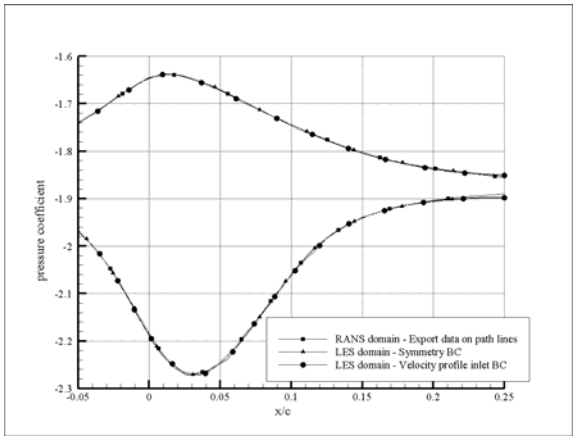

Fig. 4 Pressure-coefficient on streamlines

In order to check the validity of the simulation in 2D the pressure-coefficient (as defined in Eq.2) and the velocity component were checked in the case of the further calculation of *k-ε RANS* simulation on the RANS domain. The other two cases were initialized from the original *k-ε RANS* simulation results, but these were realized on the LES domain using symmetry BC or velocity component profiles on the streamlines (Figure 4).

3.2 Determination of the domain length in the spanwise direction

The domain was determined in wall-normal direction by a pair of streamlines and two lines being normal to the inlet flow, while the dimension of the domain along the span is to be specified by further analyses. [14] describes a well-known but not yet generalized method to characterize the spanwise dimension with cross-correlation between selected parameters. Therefore, a trial-and-error method was applied, as described in the next session.

3.3. Numerical grid

Three similar structured meshes were prepared. The difference between the grids is the spanwise extension ($L_z = 1c$, $L_z = 0.5c$ and $L_z = 0.25c$.). Each simulation has same resolution (50 cells) in the spanwise direction (Figure 5). Since this resolution is constant, therefore spanwise-streamwise aspect ratio of the cells is in inverse proportion to the extension of the domain. The domains were meshed using an O-H structure using 2.006.150 hexahedron cells, the O type being used for the vicinity of the airfoil.(Figure 6) The grid resolution on the airfoil is 237 points. The mesh was successively refined in the direction to the walls by an expansion ratio of approximately 7% (6.5% - 7.8%) to enable an accurate resolution of the boundary layer. The wall normal size of the first cells around the airfoil is linearly increasing along the chord (both on the SS and PS), starting from the leading edge of $10^{-5}c$ increasing to $2 \cdot 10^{-5}c$ at the trailing edge. This resolution corresponds to cell sizes in wall units (y^+) less than 1 in the case of 99% of the cells (Figure 7) .The equiangle skewness of none of the cells exceeds 0.67, which is appropriate for the numerical schemes used in this study. The volume ratio of adjacent cells is smaller than 1.64 in the domain.

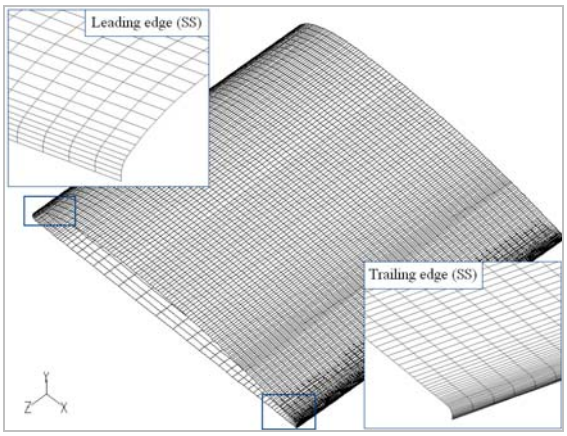

Fig. 5 Grid on the airfoil (zoomed on SS)

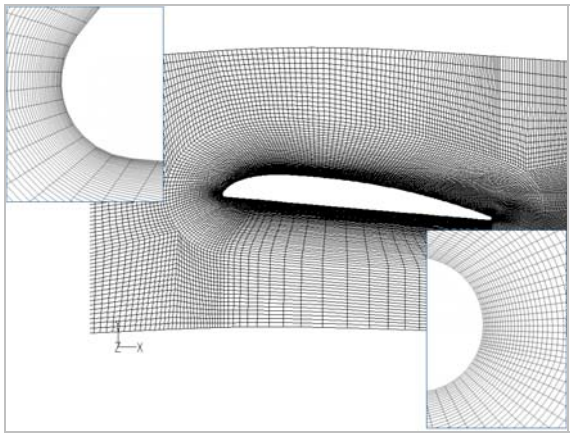

Fig. 6 2D cross-section of the grid

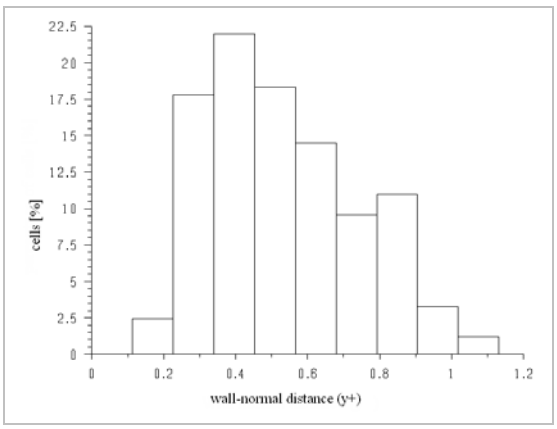

Fig. 7 Normal wall distance on the airfoil

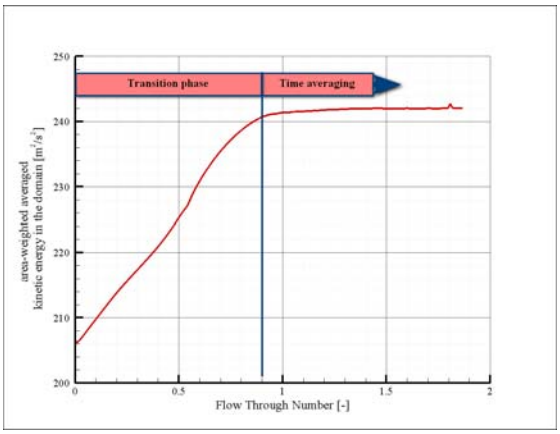

Fig. 8 Kinetic energy evaluation

3.4. Boundary conditions

As it was mentioned in the previous section, the inlet BC and outlet BC were set along a line being normal to the inlet flow. On the inlet BC, a velocity profile was set which is provided from the 2D *k-ε RANS* simulation. The inlet was free from any perturbation. This case is corresponding to an axial flow fan without any inlet guide vane, when it sucks from the open air. On the outlet BC, all diffusion terms in the normal direction were set zero, while the velocity and the pressure are extrapolated from the domain. This BC is called outflow in ANSYS FLUENT [15]. Along the streamlines, symmetry BC was chosen as it was mentioned before in the theory section. Periodic BCs were applied in the spanwise direction. This BC is used for modelling the spanwise infinite airfoil. Non-slip wall BC was applied on the wall of the airfoil. The BCs are shown in Figure 2.

3.5. Solver description and setup

In order to calculate the flow field, the commercial flow solver ANSYS FLUENT is employed for the CFD analyses. It is a finite volume solver using cell centred collocated variable arrangement, implemented for unstructured grid. For the present constant density simulation, the segregated solver was used for the sequential solution of the governing equations. To minimize the effect of the spatial discretization error, bounded central differencing scheme (BCD) was adopted for convective terms of the momentum, while the pressure in the momentum equation was discretised with standard first-order scheme. The pressure and velocity coupling in the momentum equation was absolved with the fractional step method (FSM) based on the approximation of factorization [15]. The time discretization was realised with the non-iterative time-advance (NITA) scheme. This scheme was stable during all of the simulation, and it saved approximately the 75% of the time of the simulation in contrast to the iterative time-advance scheme using the inner circle of the iteration.

The turbulence modelling was realized with the LES approach, based on the Smagorinsky Subgrid-Scale model using the dynamic approach [16, 17]. The time step for all of the simulation is set to match the required aerodynamic time resolution, to follow the Courant-Friedrichs-Lewy (CFL) criteria. The time step was $3.6 \cdot 10^{-6}$s. The maximum CFL number was smaller than 0.9 for every cases in each time instance.

Instead of using the time step to characterize the running time, the non-dimensional flow through number (FTN) is introduced. FTN is based on the time needed for a particle of velocity U_{ref} to travel from the inlet of the domain to its outlet. This value is computed as.

$$FTN = \frac{t_{flow} U_{ref}}{L} \tag{1}$$

During the simulation the cell area weighted kinetic energy was monitored (Figure 8), to monitor the temporal laminar to turbulent transition of the flow in the domain. This evaluation shows the fully developed character of the flow after approximately 1 FTN, when time-averaging was switched on. Beside this time averaging, spatial averaging was applied in spanwise direction, for further evaluation. This process provides that the results are comparable with measurement data.

4. RESULTS AND VALIDATION

The postprocessing is based on the fluctuating component of the resolved Reynolds stress tensor (RST) as well as on the time averaged pressure and on a component of the averaged velocity. The instantaneous flow parameters were analysed and the time- and

spanwise-averaged results were validated as well. The averaged simulation time was 13FTN.

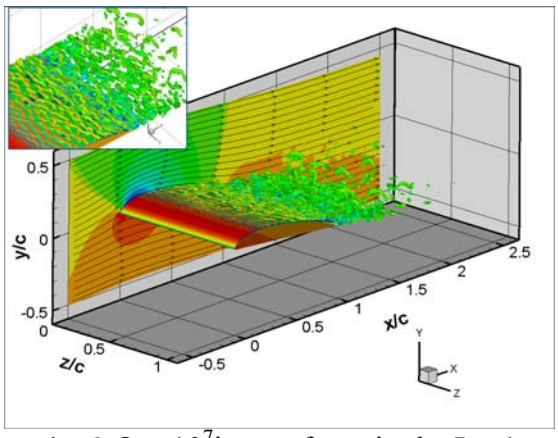

Fig. 9 Q = 10^7iso-surfaces in the L_z=1*c* domain

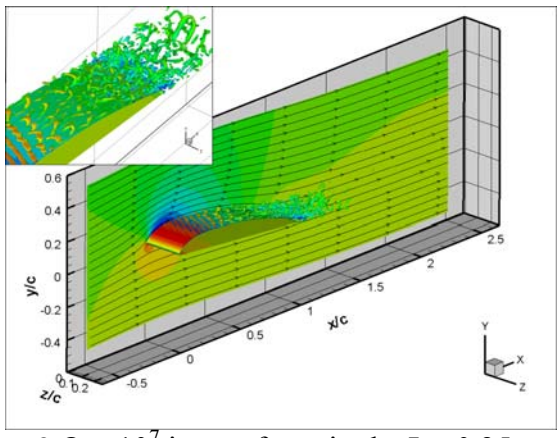

Fig. 10 Q = 10^7 iso-surfaces in the L_z=0,25*c* domain

To visualize the coherent structures in the flow field, the Q-criteria [18], i.e. setting threshold on the second invariant of the velocity gradient tensor is applied to the instantaneous flow field. Figure 9-10 presents the instantaneous Q iso-surfaces colored by the instantaneous velocity-magnitude and the instantaneous static pressure on the periodic BC in the case of L_z = 1*c* and L_z = 0,25*c* domain. The iso-surface of Q at 10^7 shows the development of three-dimensional Λ-structures after x/c = 0.3, in the case of the L_z = 0.25*c*. These structures can not be recognised on the L_z = 1*c* domain simulation, this is a clear indication of the grid dependency of the result (more details in 4.2 section). Similar grid dependency of the coherent structures was found by [19].

4.1. Pressure field validation

For comparison of the pressure distribution on the airfoil, the static pressure-coefficient has been defined as follows:

$$c_p = \frac{p - p_{ref}}{\frac{\rho}{2} U_{ref}^2}, \tag{2}$$

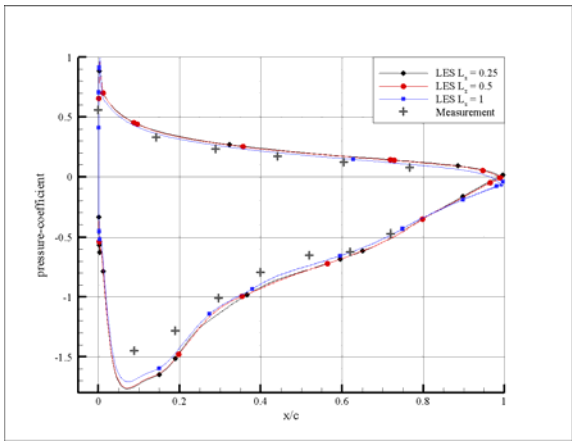

Fig. 11 Pressure-coefficient

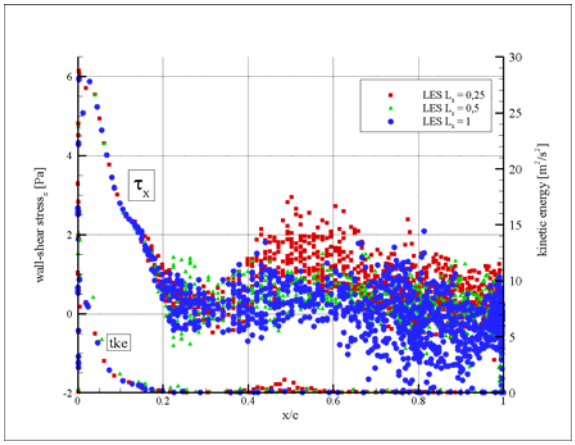

Fig. 12 Streamwise wall-shear stress (τ_x) and kinetic energy (tke)

The reference pressure is the averaged pressure on the inlet of RANS domain, along normal to the streamwise direction. The reference velocity is equal to the velocity value at the inlet of the LES domain boundary. The comparison of the computed static pressure coefficient profiles against the measurement is shown in Figure 11. A remarkably good agreement was found and the local minimum shows the most confined part of the cross section above the airfoil. However, the boundary layers on the walls of the wind tunnel are present in the measurement but are completely neglected in the simulations.

4.2. The laminar to turbulent transition

The transition can be both deduced from the kinetic energy development and the spanwise wall shear stress component. As Figure 12 demonstrates, the first local minimum in the shear stress data cloud coincides with the beginning of the transition zone ($x \approx 0.2c$), and the extensive spread of the points show the fully turbulent zone [20]. Figure 13 shows the evaluated spanwise wall shear stress waves on the front part of 1/3 chord of airfoil SS surface, which indicates the transition zone. During the measurements separation was suggested with the flow visualization techniques, but in the case of averaged flow pattern of simulation the separation could not recognized. The separation phenomenon and the transition are the objects of further analyses.

The patterns on the last 1/3 chord SS of the airfoil suggest the grid dependency of the shear stress distribution. This grid dependency indicates also further analyses with constant spanwise resolution on more narrowed domain and on double wide domain of $L_z=0.25c$.

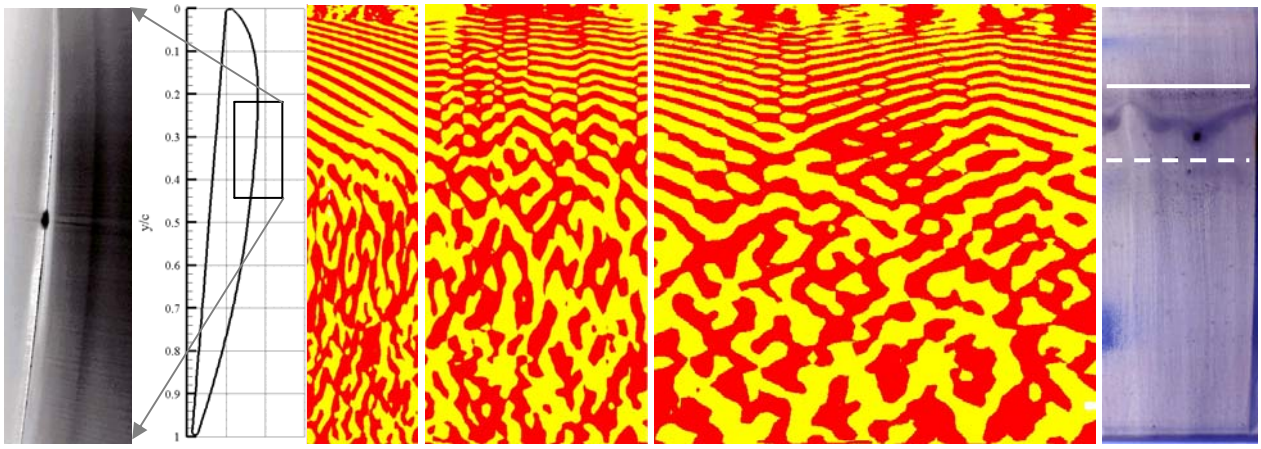

a.) b.) c.) d.) e.)

Fig. 13 a.) Flow visualisation using laser sheet above SS, showing separation (inverted colours),
b.) Wall-shear stress in spanwise (τ_z) on $L_z = 0.25c$ domain,
c.) Wall-shear stress in spanwise (τ_z) on $L_z = 0.5c$ domain,
d.) Wall-shear stress in spanwise (τ_z) on $L_z = 1c$ domain,
e.) Separation zone in NPL measurement with oil flow visualisation. Line nominates the separation, dashed lines nominates the reattachment (inverted colours).

4.3. Velocity field validation

The velocity field validation is based on the six lines being perpendicular to the SS surface of the airfoil, and three lines being perpendicular to the streamwise direction in the wake of the airfoil, at $1.1c$, $1.25c$ and $1.5c$ (Figure 14) and one being upstream of the airfoil. In order to transform the results into the airfoil local coordinate-system, the rotation matrix was applied, and the results are presented in the local coordinate-systems. The computed velocity profiles show a good agreement with the LDA measurement data downstream the

leading edge, upstream the trailing edge and in the wake. Downstream of the transition zone the simulation over predicts the velocity out of the boundary layer. From the three simulations, the one related to the domain of L_z=0.25*c* shows the best agreements with the measurement even in the x=*0,98c* point, where the difference is still approximately 40%. Unfortunately, no experimental data is available in the bottom zone of the boundary layer. It is well known that the difficulties of the measurement near the trailing edge because of the vortices. Each LES simulations accurately estimate the profiles in the wake in the case of magnitude values and the position of the minimum of the velocity value in the wake.

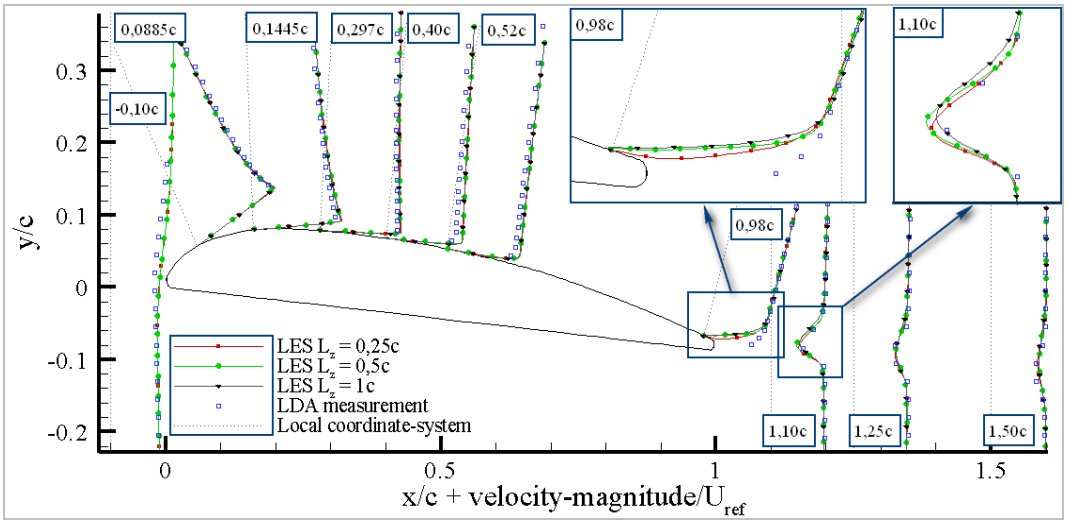

Fig. 14 Velocity profiles validation along local coordinate-system of the lines

4.4. Velocity fluctuation validation

The LDA studies provided one component turbulence intensity data, but in the numerical simulation every elements of the RST can be calculated (Eq 4.). The fluctuation of the streamwise velocity (u_{rms}) can be calculated from the Eq.3:

$$u_{rms} = \frac{TuU_{ref}}{100}. \qquad (3)$$

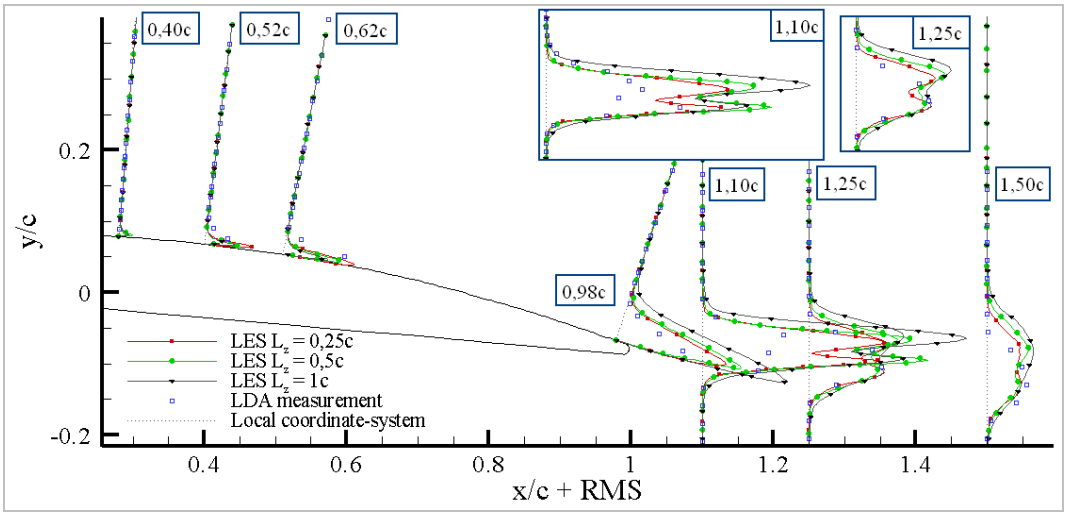

Fig. 15 Fluctuation of component of the streamwise and wall-normal velocity along local coordinate-system of lines. ▲ $L_z = 1c$, ● $L_z = 0.5c$, ■ $L_z = 0.25c$

In the case of the simulation the fluctuation is defined in Eq.4 using the RST component.

$$u_{rms} = (\overline{u'})(\overline{u'}) - \overline{u'u'} \,. \tag{4}$$

The averaged fluctuation value is shown in the local coordinate-system of the postprocessing lines on the SS and in the wake in Figure 15. The fluctuation of the streamwise velocity and wall-normal velocity are underestimated above the boundary layer of the SS until x = 0.62*c*. On the line of x = 0.98*c* position the rms is over predicted in each simulation, which is coinciding with the non-dimensional velocity differences at the same position. Focusing on the x = 0.98*c* position and the results in the wake, it can be seen in Figure 15 that the domain reduction in the spanwise direction is in directly proportion to the accuracy of the simulations to the measurements, i.e. results on narrower domain are closer to the measurements.

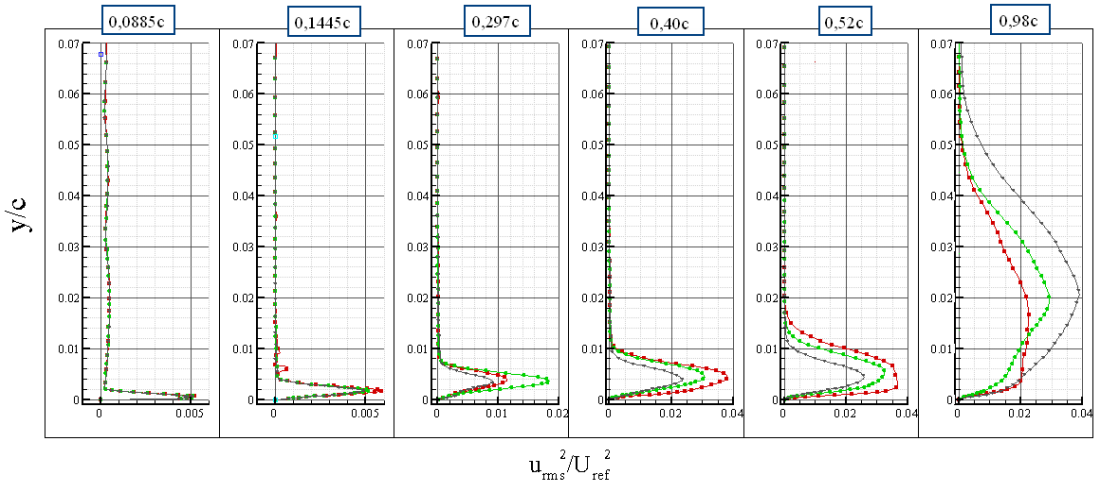

Fig. 16 Non-dimensional fluctuation of x-velocity, ▲ $L_z = 1c$, ● $L_z = 0.5c$, ■ $L_z = 0.25c$

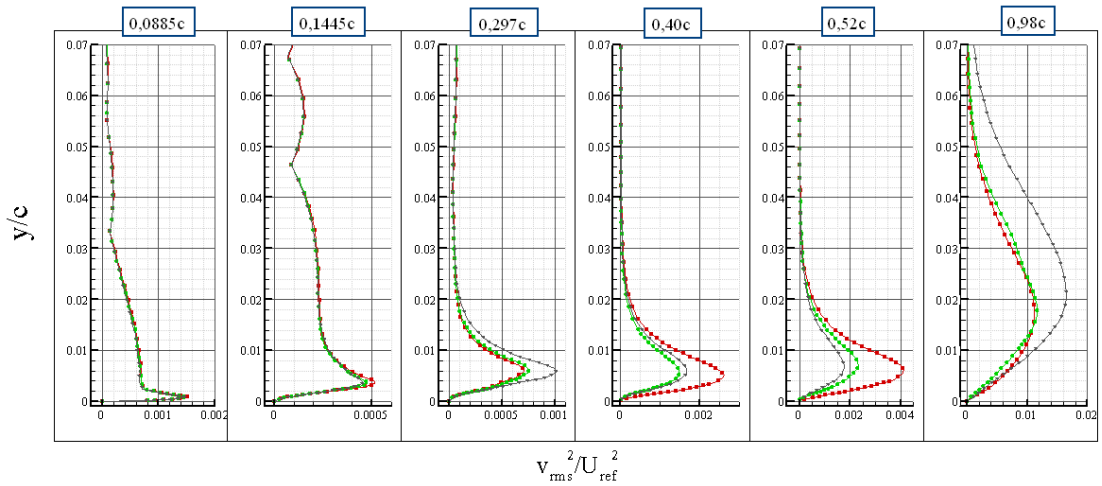

Fig. 17 Non-dimensional fluctuation of y-velocity, ▲ $L_z = 1c$, ● $L_z = 0.5c$, ■ $L_z = 0.25c$

To see how the domain size change affected the turbulence anisotropy the fluctuation of the x, y and z velocities are presented in Figure 16-18. All the three components are showing the similar sequential decrease tendency as it shows in Figure 15. After the beginning of the transition (x ≈ 0.2*c*), the streamwise fluctuation is increased with one order of magnitude. The rms of the y-velocity is smaller than rms of the x-velocity with one order of magnitude. The

thickness of the boundary layer can be also read from Figure 16 and Figure 18. The domain reduction is resulted in increase of all normal Reynolds stress components except close to the trailing edge where the trend is the opposite; the production of turbulence in the turbulent part of the SS is enhanced by size reduction but reduced close to the trailing edge.

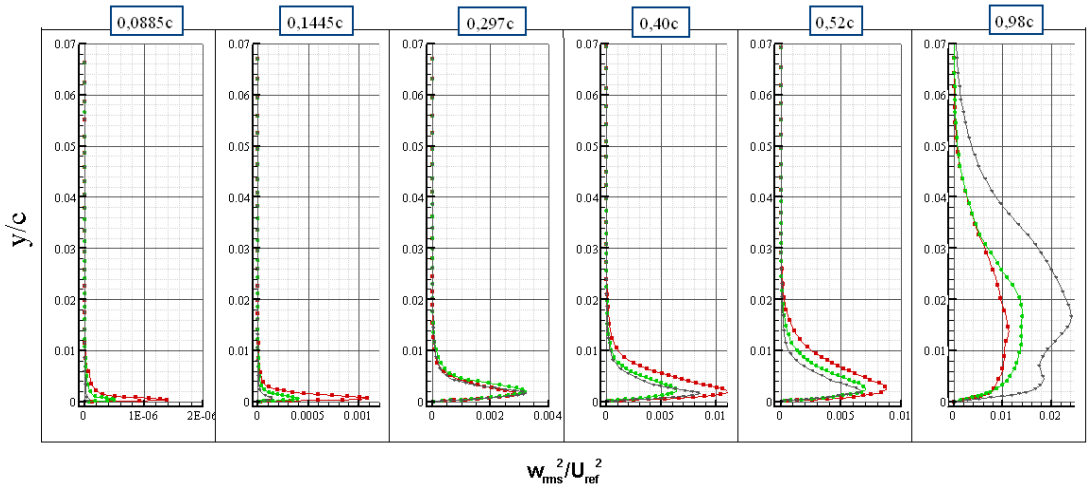

Fig. 18 Non-dimensional fluctuation of z-velocity, ▲ $L_z = 1c$, ● $L_z = 0.5c$, ■ $L_z = 0.25c$

5. CONCLUSIONS

This was the first study in the DFM using Hybrid/Zonal RANS/LES method. The commercially available ANSYS FLUENT was employed, and it was validated with in-house LDA and pressure measurement in the NPL type wind tunnel. The qualitative validation was realised through oil flow and laser sheet visualisation and the separation region on the SS of the airfoil was shown. However, the major problem is the resolution in the spanwise direction. The $L_z = 0.25c$ simulation was showing the best agreement with the measurement and in this case characteristic Λ structure was reached above the SS of the airfoil. The future work covers the separation and the transition analyses on domain and the grid dependency.

ACKNOWLEDGEMENT

This work has been supported by the Hungarian National Fund for Science and Research under contract No. OTKA K63704.

NOMENCLATURE AND SUBSCRIPT

c	[m] chord length	t	[s] simulation time
c_p	[-] pressure-coefficient	y^+	[-] dimension wall distance
k	[m^2s^{-2}] turbulent kinetic energy	z	[m] coordinate in spanwise
L	[m] domain spanwise extension		
p	[Pa] static pressure	ν	[m^2s^{-1}] kinematic viscosity
t	[s] flow time	ε	[m^2s^{-2}] dissipation rate
Tu	[%] turbulent intensity	ρ	[kgm^{-3}] density
U	[ms^{-1}] streamwise velocity comp.	ω	[$1s^{-1}$] specific dissipation rate
V	[ms^{-1}] wall-normal direction velocity comp.	$\bar{u}$	averaged parameter
W	[ms^{-1}] spanwise velocity component	rms, `	fluctuation
x	[m] coordinate in streamwise	ref	reference
y	[m] coordinate in wall-normal		

LIST OF ABBREVIATIONS

BC	Boundary condition
BCD	Bounded central differencing scheme
BME	Budapest University of Technology and Economics
CAA	Computational aeroacoustics
CFD	Computational fluid dynamics
CFL	Courant Friedrichs Lewy
DFM	Department of Fluid Dynamics
DNS	Direct numerical simulation
FSM	Fractional step method
FTN	Flow through number
LDA	Laser-Doppler Anemometer
LES	Large-eddy simulation
NITA	Non-iterative time advanced
NPL	National Physics Laboratory
PISO	Pressure-implicit with splitting of operators
PS	Airfoil pressure side
RANS	Reynolds averaged Navier-Stokes equations
RST	Reynolds stress tensor
SS	Airfoil suction side
SST	Shear-stress transport

REFERENCES

[1] Nagy L, Lohász MM, Vad J. RANS simulation of RAF6 airfoil, Gépészet2006 Conference, Budapest, 2006
[2] Nagy L. Development of a methodology for the noise prediction of a rotating object, Project Report 2007-18, von Karman Institute for Fluid Dynamics, Rhode-Saint-Genese, 2007
[3] Carolus T, Schneider M, Hauke R. Axial flow fan broad-band noise and prediction, Journal of Sound and Vibration vol. 300 pp. 50-70, 2007
[4] Jang CM, Masato F, Inoue M. Frequency characteristics of fluctuating pressure on rotor blade in a propeller fan. JSME International Journal Series B. Vol. 46 No. 1 pp. 163-172, 2003
[5] Tsuchiya N, Nakamura Y, Goto S, Kodama H, Nozaki O, Nishiazawa T, Yamamoto K. Low noise FEGV designed by numerical method based on CFD, Proceeding of ASME Turbo Expo 2004, June 14-17, Vienna, Austria, 2004
[6] Cavus M, Sorgüven E, Arslan E, Misirlioglu A. Aeroacoustic noise prediction of an axial fan in a circular duct with LES, AIAC Proceedings, AIAC-2005-092, 2005
[7] Davidson L, Billson M. Hybrid LES-RANS using synthesized turbulent fluctuations for forcing in the interface region Heat and Fluid Flow vol. 27 pp. 1028-1042, 2006
[8] Keating, A, De Prisco G, Piomelli U.Interface conditions for hybrid RANS/LES calculations, Heat and Fluid Flow vol. 27 pp. 777-788, 2006
[9] Labourasse E, Sagaut P. Reconstruction of turbulent fluctuations using a hybrid RANS/LES approach. J. Comput. Phys., vol. 182 pp. 301-336, 2002.
[10] Terracol M, Manoha E, Herrero C, Labourasse E, Redonnet S, Sagaut P. Hybrid methods for airframe noise numerical prediction. Theoretical and Computational Fluid Dynamic vol. 19 pp. 197-227, 2005
[11] Patterson GN. Ducted Fans. Design for High Efficiency. Australian Council for Aero. Rep. ACA 7, 1944
[12] The Department of Aerospace Engineering at the University of Illinois at Urbana-Champaign (UIUC), Airfoil database http://www.ae.uiuc.edu/m-selig/ads/coord_database.html#R (15 March 2008)
[13] Vad J, Koscsó G, Gutermuth M, Kasza Zs, Tábi T, Csörgő T. Study of the aero-acoustic and aerodynamic effects of soft coating upon airfoil JSME International Journal Series C-Mechanical Systems Machine Elements and Manufacturing, vol 49(3), pp. 648-656, 2006
[14] Davidson L, Fröhlich J, Mellen C. LESFOIL: Large Eddy Simulation of Flow Around a High Lift Airfoil Springer, pp.135-147, 201-222, 2003
[15] Fluent Inc. Fluent 6.3 User's Guide, Lebanon, New Hampshire 2006
[16] Germano M; Piomelli U; Moin P, Cabot WH. A Dynamic Subgrid-Scale Eddy Viscosity Model, Physics of Fluids A-Fluid Dynamics, vol 3(7), pp. 1760 - 1765. 1991
[17] Kim SE. Large Eddy Simulation Using Unstructured Meshes and Dynamic Subgrid-Scale Turbulence Models 34th AIAA Fluid Dynamics Conference and Exhibit, Portland Oregon, 2004
[18] Hunt JCR, Wray AA, Moin P. Eddies, streams, and convergence zones in turbulent flows, Center for Turbulence Research, Annual Research Briefs, pp. 193-202, 1988
[19] Tóth P, Lohász MM. Grid dependency experiments of the Kelvin-Helmholtz vortices in Large-Edd Simulation, Proceeding of the microCAD 2008 international Scientific Conference, pp. 61-66. 2008
[20] Boiko AV, Grek GR, Dovgal AV, Kozlov VV. The origin of turbulence in near-wall flows. Springer ISBN 3-540-42181-5, 2002